

# Cu–Zn–Cr<sub>2</sub>O<sub>3</sub> Catalysts for Dimethyl Ether Synthesis: Structure and Activity Relationship

Akula Venugopal · Jelliarko Palgunadi ·  
Kwang Deog Jung · Oh-Shim Joo · Chae-Ho Shin

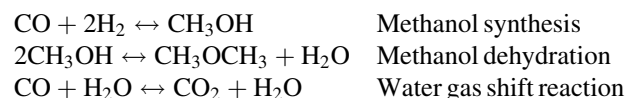
Received: 11 December 2007 / Accepted: 18 January 2008 / Published online: 12 February 2008  
© Springer Science+Business Media, LLC 2008

**Abstract** The CuO dispersed on ZnCr<sub>2</sub>O<sub>4</sub> catalysts derived from Cu–Zn–Cr hydrotalcite like layered double hydroxide precursors with varying Zn/Cr ratios have been synthesized, characterized by BET—Surface area, X-ray diffraction (XRD), temperature programmed reduction (TPR), electron spin resonance (ESR), N<sub>2</sub>O titrations and the activities were evaluated for single step dimethyl ether (STD) synthesis from syngas. It is observed that the copper species were in highly dispersed state over Cu–ZnO–Cr<sub>2</sub>O<sub>3</sub> at high Zn/Cr ratios while the copper cluster were present at low Zn/Cr ratios. The ESR analysis revealed signals due to isolated Cu<sup>2+</sup> at high Zn/Cr ratios and clustered Cu<sup>2+</sup> at low Zn/Cr ratio in fresh catalysts and only Cr<sup>3+</sup> species in used catalysts. The TPR results indicated that the reduction peak shifted to high temperatures with an increase in chromium content due to large copper crystallites, which was supported by XRD analysis. The conversion of syngas to DME was well correlated with the copper metal surface areas, indicating that STD synthesis can be controlled by methanol synthesis rate.

**Keywords** Cu–Zn–Cr · Hydrotalcite · Dimethyl ether · Cu metal surface area · Syngas · N<sub>2</sub>O decomposition

## 1 Introduction

Single step dimethyl ether synthesis from syngas is mainly composed of methanol synthesis, methanol dehydration and water gas shift reaction.



Single step dimethyl ether synthesis from syngas has technological advantages over the two step process of methanol synthesis and the following methanol dehydration. The advantages being (1) high one-through conversion in thermodynamic point of view [1] and (2) low operating cost in the economic point of view [2]. The STD synthesis has been conducted on the admixed catalysts of methanol synthesis and methanol dehydration. For the STD synthesis, the methanol synthesis catalysts were chosen from Cu/Zn oxides dispersed on Al<sub>2</sub>O<sub>3</sub> and/or Cr<sub>2</sub>O<sub>3</sub> systems, while methanol dehydration is carried out over solid acid catalysts [3–6]. The effects of solid acid catalysts on STD synthesis from syngas were studied with the admixed catalysts of Cu/ZnO/Al<sub>2</sub>O<sub>3</sub> and ZSM-5 [7]. However, STD synthesis rates are not dependent on the acidity of the solid acid catalysts, but on the amount of methanol synthesis catalysts in the admixed catalysts, although methanol dehydration rate is closely proportional to the acidity of the solid acid catalysts. Therefore, it is suggested that the STD reaction rate on the admixed catalysts could be dependent on methanol synthesis rate, over the solid acid catalysts with moderate acid sites such as  $\gamma$ -Al<sub>2</sub>O<sub>3</sub> are used. It is in

---

A. Venugopal (✉)  
Catalysis Section, Indian Institute of Chemical Technology,  
Hyderabad 500 007, India  
e-mail: akula@iict.res.in

J. Palgunadi · K. D. Jung (✉) · O.-S. Joo  
Hydrogen Energy Research Center,  
Korea Institute of Science and Technology,  
P.O. Box 131, Cheongryang, Seoul, Korea  
e-mail: jkdcacat@kist.re.kr

C.-H. Shin  
Department of Chemical Engineering,  
Chungbuk National University, Gaseshindong 48,  
Heungdukgu, Cheongju, Seoul 361-763, Korea

general agreement that methanol synthesis rates are proportional to Cu metal surface areas, although the higher activity of Cu–Zn based catalysts for methanol synthesis has been studied for several decades in the aspects of electronic properties of Cu and ZnO [8], stabilizations of special morphologies [9, 10], spillover phenomena [11–14], and specific interaction at the Cu/ZnO interface [15]. It is reported that methanol synthesis rates are linearly proportional to Cu surface areas irrespective of the supports [16]. Another important aspect is the synergistic effect of Cu and ZnO are suggested for methanol synthesis. Nevertheless, it is shown that linear correlations of rate of methanol synthesis with Cu metal surface areas are obtained but the slopes of the curves dependent upon the support material [17–20]. The stability of Cu/ZnO catalysts has been discussed in view of the sintering of Cu via brass formation [21–24]. It is suggested that the sintering of Cu via brass formation could be prevented in Cu–Zn–Cr hydrotalcite-like precursors [25]. Thermally stable catalysts are required because STD synthesis is highly exothermic reaction as compared to methanol synthesis. Therefore, Cu–Zn–Cr catalytic systems prepared by the hydrotalcite-like precursor are used for STD synthesis in this study. It is generally known that precursors of copper containing hydrotalcites are very sensitive towards thermal treatments and the copper dispersion is dependent upon the preparation conditions such as pH, Zn/Cr ratios and dispersing agent. This paper illustrates the synthesis and characterization of Cu on ZnO–Cr<sub>2</sub>O<sub>3</sub> matrix derived from the Cu–Zn–Cr layered double hydroxide (LDH) precursors. A series of Cu–ZnO–Cr<sub>2</sub>O<sub>3</sub> (with Zn/Cr = 1.2–6.8) catalysts have been synthesized and characterized. The conversions of CO to DME synthesis are evaluated on the admixed catalysts composed of Cu–Zn–Cr and  $\gamma$ -Al<sub>2</sub>O<sub>3</sub>.

The physico-chemical properties of Cu–ZnO–Cr<sub>2</sub>O<sub>3</sub> catalysts, which were elucidated by BET—surface area, X-ray diffraction (XRD), electron spin resonance (ESR), temperature programmed reduction (TPR) analyses, and N<sub>2</sub>O titrations are very well correlated with the conversion of syngas to DME.

## 2 Experimental

### 2.1 Catalyst Preparation

Cu–Zn–Cr hydrotalcite-like precursors were prepared by coprecipitation method with constant Cu and various Zn/Cr mole ratios in order to investigate its influence on copper dispersion, since the copper particles are dispersed and stabilized by ZnO and Cr<sub>2</sub>O<sub>3</sub>. In a typical method, required amounts of copper, zinc and chromium nitrate salts were

dissolved in 600 mL of distilled water (solution A) and a solution B containing 2 M NaOH and 1 M Na<sub>2</sub>CO<sub>3</sub> (1:1 = v/v) were added simultaneously to 2.0 L of distilled water under vigorous stirring. The mole ratios of Cu:Zn:Cr of the prepared catalysts denoted as CZC were 7:6:0.88 (CZC-6.8), 7:5.3:1.6 (CZC-3.3), 7:4.6:2.4 (CZC-1.9), 7:3.8:2.7 (CZC-1.4) and 7:3.6:2.9 (CZC-1.2) respectively. The CZC-X indicates the mole ratio of Zn/Cr = X. A constant pH  $\sim$  8.9 is maintained while adjusting the flows of solution A and solution B during the co-precipitation of the samples. The coprecipitation was carried out at room temperature and the precipitate was aged for 1 h, washed several times until pH of the gel reached the pH of the distilled water. The residual Na concentration is found to be <0.03% by atomic absorption spectroscopy. The resulting precipitate was filtered, oven dried at 100 °C for 24 h and calcined in static air at 400 °C/3 h at a ramping rate of 4 °C/min. For the comparison, the Zn–Cr (Zn:Cr = 3:1 mol ratio) and Cu–Cr (Cu:Cr = 1:1 mol ratio) samples were prepared under similar conditions adopted as mentioned above [26].

### 2.2 Characterization

The BET-surface areas of the calcined catalysts were obtained by means of dinitrogen physisorption at ca. 77 K using a Micromeritics ASAP 2000 instrument. Prior to the measurements, the catalysts were degassed at 120 °C for 0.5 h. The X-ray diffraction analysis of the oven dried and calcined samples were carried out in the  $2\theta$  range from 5 to 90° using a Rigaku Diffractometer employing Ni filtered Cu K <sub>$\alpha$</sub>  radiation at 40 kV and 126 mA. The temperature programmed reduction (TPR) and the N<sub>2</sub>O decomposition were carried out using a fixed bed reactor connected to a GC with thermal conductivity detector. For TPR analysis 5% dihydrogen in Ar was used. In case of N<sub>2</sub>O titrations, Porapak N column was used for the N<sub>2</sub>O and N<sub>2</sub> separation. About 30–80 mg of catalyst loaded was reduced in 5% H<sub>2</sub>/Ar stream at 250 °C for 1 h and the N<sub>2</sub>O titrations were carried out at 90 °C. Several replicate experiments were carried out and the averaged value was chosen for Cu metal surface areas. In this investigation, a surface copper density of  $1.46 \times 10^{19}$  atoms/m<sup>2</sup> was used for the copper metal area calculations [27]. The Electron Spin Resonance (ESR) analysis was performed at room temperature using JEOL, JES-FA200 ESR spectrophotometer by X-band equipment with an operating frequency  $\nu = 9.029$  GHz.

### 2.3 Activity Measurements

DME synthesis was carried out using a fixed bed micro reactor loaded with finely mixed catalysts composed of

0.5 g of activated methanol synthesis catalyst (Cu–Zn–Cr) and 0.5 g of methanol dehydration catalyst i.e.  $\gamma$ -Al<sub>2</sub>O<sub>3</sub>. Prior to the reaction the catalysts were reduced in a stream of 5% H<sub>2</sub>/Ar in a sequential reduction steps as follows: 1st step: treatment at 100 °C/0.5 h, 2nd step: reduction at 180 °C/0.5 h, 3rd step: reduction at 240 °C/2 h, 4th step: reduction at 280 °C/0.5 h. The activity of the catalysts for the STD synthesis was tested under the reaction conditions of the H<sub>2</sub>–CO ratio of 1.5, a GHSV of 6000 h<sup>-1</sup>, pressure of 600 psig and the reaction temperature ranges from 240 to 270 °C. The reaction mixture was passed through a purifier in order to eliminate traces of water, oxygen and iron carbonyl that would deactivate the catalyst. The effluent gas mixture was analyzed by an on-line gas chromatograph equipped with thermal conductivity detector using Porapak Q column. The experimental error in the evaluation of the catalysts was found to be  $\pm 2\%$  unless otherwise mentioned.

### 3 Results

#### 3.1 Activity Dependence on Copper Metal Surface Area

DME synthesis rates on the admixed catalysts of the prepared Cu/ZnO/Cr<sub>2</sub>O<sub>3</sub> and  $\gamma$ -Al<sub>2</sub>O<sub>3</sub> were plotted with respect to Cu surface areas as shown in Fig. 1. The STD reaction rates,  $r_{\text{CO}}$  increased proportionally with Cu metal surface area, suggesting that the DME synthesis rates are directly proportional to the copper metal surface area. In previous results, DME synthesis rates increased with an increase in amounts of Cu in Cu/ZnO based catalysts in the

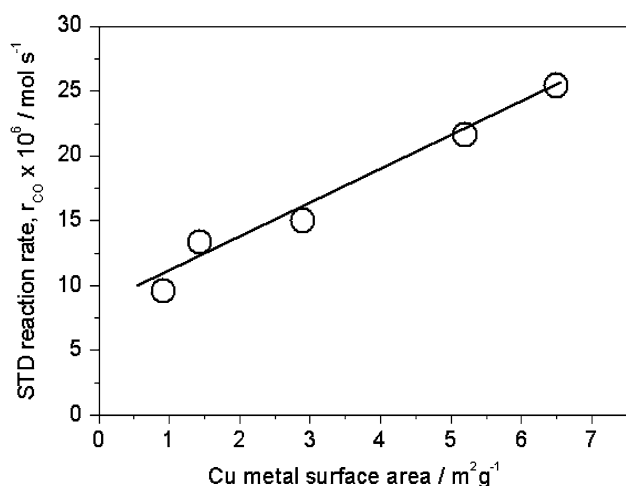


**Fig. 1** The relationship between syngas conversion and copper metal surface area measured by N<sub>2</sub>O titrations

admixed catalysts [7]. This increase is found to be equivalent to the increase in specific Cu surface areas of the admixed catalysts. There is general agreement that rate of methanol synthesis is well correlated with Cu surface area, although one slope independent on Cu supports was suggested by some authors and different slopes dependent on Cu supports were done by the other authors [28]. Therefore, this experimental result supports that the STD reaction rate on the admixed catalysts could be dependent on methanol synthesis rate. It means that methanol synthesis rate on Cu–Zn–Cr<sub>2</sub>O<sub>3</sub> catalyst part in the admixed catalysts can be much lower than methanol dehydration on  $\gamma$ -Al<sub>2</sub>O<sub>3</sub> part in STD synthesis reaction.

#### 3.2 BET Surface Area and XRD Analysis

The BET surface areas of the calcined samples, the crystalline phases of the oven dried and calcined samples of Cu–Zn–Cr catalysts, and Cu metal surface areas by N<sub>2</sub>O titration are reported in Table 1. The BET surface areas of Cu–Zn–Cr<sub>2</sub>O<sub>3</sub> catalysts are in the range of 41.4–63.6 m<sup>2</sup>/g and no dependency of the BET surface areas on the ratios of Zn to Cr is found. The XRD patterns of the oven-dried samples reveal the diffraction lines of Cu–Zn–Cr LDH structure as shown in Fig. 1 [29, 30]. The XRD patterns show the decrease of crystallinity with an increase in chromium loading. At high Zn/Cr ratios the diffraction lines were intense and sharp. The intensities of Cu–Zn–Cr HT peaks increased with an increase in Zn concentration and Frost and Ding report similar phenomenon at high zinc concentration over Cu–Zn–Cr HT samples [31]. For comparison purpose, the Zn–Cr (mole ratio = 3/1) and Cu–Cr (mole ratio = 1/1) are also prepared under identical preparation conditions and their diffraction patterns are shown in Fig. 2. Presence of CuO phase in oven dried samples is ascribed to the Jahn-Teller effect due to the deviant behavior of copper when the Cu/Zn ratio >1 is maintained in the ternary Cu–Zn–Cr catalysts [32].

XRD patterns of the calcined samples are shown in Fig. 3 and the observed phases are reported in Table 1. The HT structure of Cu–Zn–Cr collapsed upon thermal decomposition in air at 400 °C/3 h. Phases due to CuO [ICDD: 80-0076] and ZnO [ICDD: 89-1397] are predominant and the ZnCr<sub>2</sub>O<sub>4</sub> phase [ICDD: 22-1107] is minor in intensity. It is also observed that some of the diffraction lines of ZnO and ZnCr<sub>2</sub>O<sub>4</sub> are superimposed. The intensities of CuO and ZnO peaks increased with an increase in Zn/Cr ratio up to 1.9 and the ZnO characteristic peaks were predominant at Zn/Cr ratio higher than 1.9. This indicates the high interaction between CuO and ZnO particles at high Zn/Cr ratios. The very weak diffraction lines due to CuCr<sub>2</sub>O<sub>4</sub> [ICDD: 72-1212] are observed over Cu/Cr<sub>2</sub>O<sub>3</sub>

**Table 1** Physico-chemical characteristics of the Cu–Zn–Cr catalysts prepared by coprecipitation method at pH  $\sim 8.9 \pm 0.1$ , calcined in air at 400 °C/3 h

Catalyst	BET-SA (m <sup>2</sup> /g)	XRD oven dried	XRD calcined	XRD used	H <sub>2</sub> uptake (mmol/g)	S <sub>Cu</sub> (m <sup>2</sup> /g)
CZC-6.8	57.9	HT, CuO	CuO(M), ZnO(M), ZnCr <sub>2</sub> O <sub>4</sub> (m)	Cu <sup>0</sup> (m), ZnO(M), ZnCr <sub>2</sub> O <sub>4</sub> (w)	6.91	5.2
CZC-3.3	63.6	HT, CuO	CuO(M), ZnO(M), ZnCr <sub>2</sub> O <sub>4</sub> (m)	Cu <sup>0</sup> (M), ZnO(M), ZnCr <sub>2</sub> O <sub>4</sub> (w)	6.69	6.5
CZC-1.9	47.1	HT, CuO	CuO(M), ZnO(m), ZnCr <sub>2</sub> O <sub>4</sub> (m)	Cu <sup>0</sup> (m), ZnO(M), ZnCr <sub>2</sub> O <sub>4</sub> (w)	6.55	2.9
CZC-1.4	50.9	HT, CuO	CuO(M), ZnO(m)	Cu <sup>0</sup> (M), ZnO(m), ZnCr <sub>2</sub> O <sub>4</sub> (w)	6.85	1.44
CZC-1.2	41.4	HT, CuO	CuO(M), ZnO(m), CuCr <sub>2</sub> O <sub>4</sub> (m)	Cu <sup>0</sup> (M), ZnO(m), ZnCr <sub>2</sub> O <sub>4</sub> (w)	–	0.92
Zn–Cr	18.6	HT	ZnO(M), ZnCr <sub>2</sub> O <sub>4</sub> (m)	–	–	–
Cu–Cr	37.5	HT	CuO(M), CuCr <sub>2</sub> O <sub>4</sub> (m)	–	–	–

HT, Hydrotalcite-type structure

M, Major

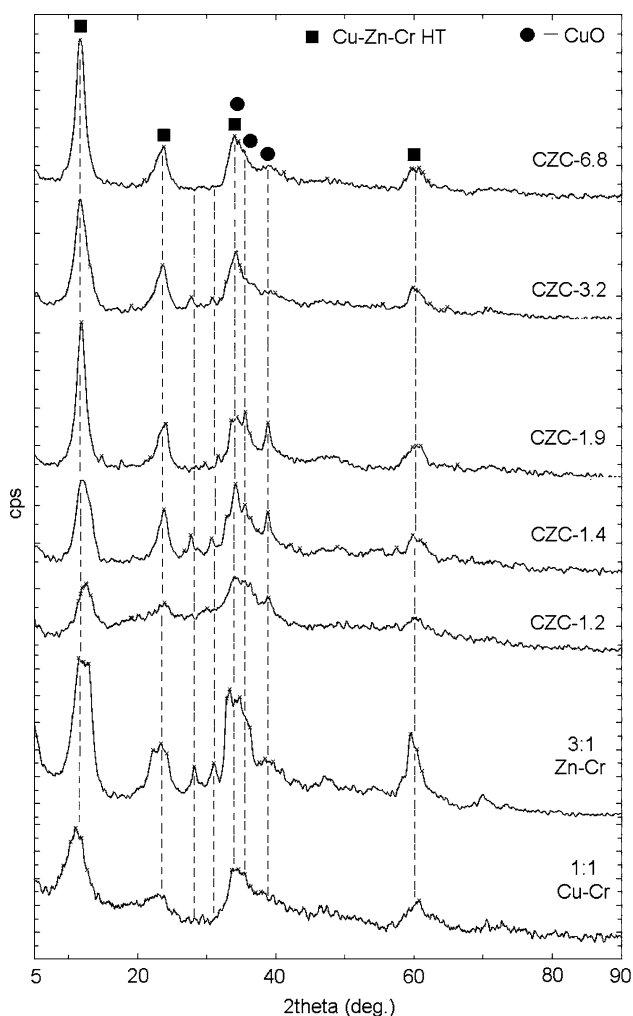
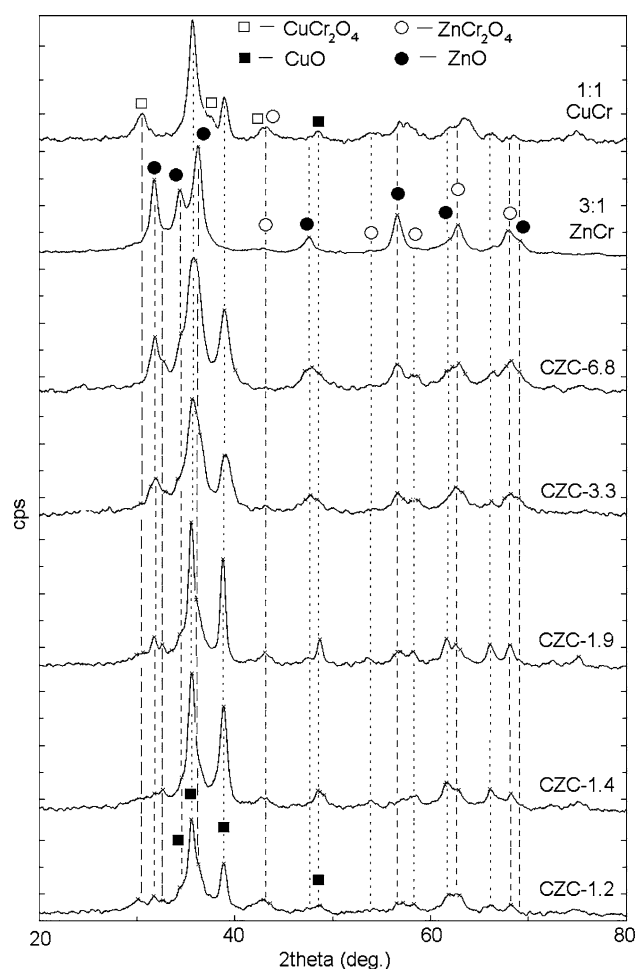
m, minor

w, weak

H<sub>2</sub> uptake, the hydrogen uptakes measured from the TPR analysisS<sub>Cu</sub>, Copper metal surface area measured by N<sub>2</sub>O titration

and the Cu/ZnO/Cr<sub>2</sub>O<sub>3</sub> (Zn/Cr mole ratio = 1.2) samples. None of the catalysts showed diffraction lines due to Cr<sub>2</sub>O<sub>3</sub> phase even at low Zn/Cr = 1.2, this is possibly due to

amorphous nature of Cr<sub>2</sub>O<sub>3</sub> or might be due to an interaction of Cr<sub>2</sub>O<sub>3</sub> with ZnO particles at high Zn/Cr and with CuO at low Zn/Cr ratios present in the catalyst [33]. From

**Fig. 2** The XRD patterns of the oven dried Cu–Zn–Cr samples**Fig. 3** The XRD patterns of the calcined Cu–Zn–Cr catalysts (CZC-X) X = Zn/Cr ratio

this it can be concluded that higher is the interaction between Cu and Zn, lesser is the possibility of Cu and/or Zn—Cr<sub>2</sub>O<sub>4</sub> formation.

After DME synthesis reactions under the condition at temperatures of 240–270 °C, at 40.8 atm, and the GHSV of 6000 h<sup>-1</sup>, the used admixed catalysts of Cu/ZnO/Cr<sub>2</sub>O<sub>3</sub> and  $\gamma$ -Al<sub>2</sub>O<sub>3</sub> are subjected to XRD analysis and their patterns are reported in Fig. 4. Diffraction lines due to metallic copper [ICDD: 85-1326] and ZnO [ICDD: 89-1397] phase are observed. The catalysts with low Zn/Cr ratios displayed strong lines due to metallic copper as compared to those with high Zn/Cr ratios. The CuO peaks in calcined samples (Fig. 3) disappeared after the syngas reaction, which is due to the reduction of Cu<sup>2+</sup>–Cu<sup>0</sup> phase [34]. It is also observed that CuCr<sub>2</sub>O<sub>4</sub> peak intensities decreased in used catalysts as compared to fresh catalysts.

### 3.3 Electron Spin Resonance analyses (ESR)

The ESR spectroscopy is used to investigate the paramagnetic species of Cu<sup>2+</sup>, Cr<sup>3+</sup> and Cr<sup>5+</sup> present in the Cu–Zn–Cr catalysts. The room temperature ESR spectra of the fresh and used catalysts are shown in Figs. 5 and 6 respectively. From Fig. 5 it is evident that the peak shapes of the signals attributed to Cu<sup>2+</sup> changed with increase in

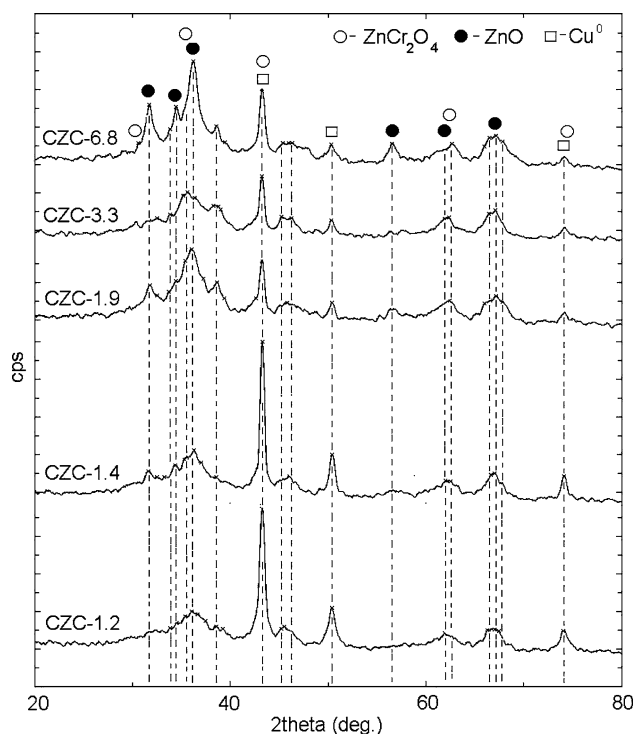


**Fig. 4** The XRD patterns of the used Cu–Zn–Cr catalysts (CZC-X) X = Zn/Cr ratio

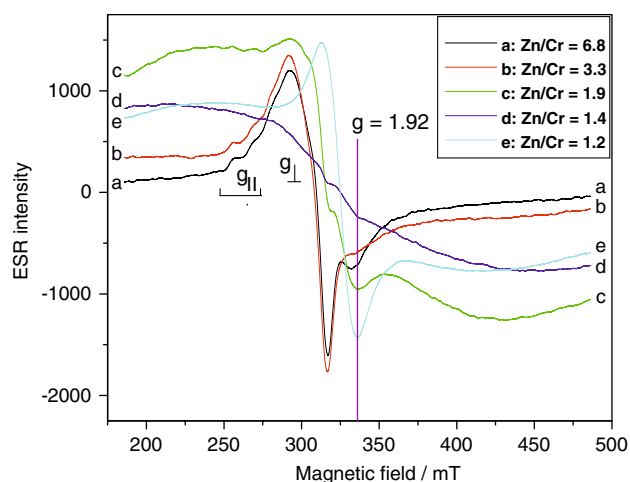


**Fig. 5** The ESR spectra of the calcined catalysts; (a) CZC-6.8, (b) CZC-3.3, (c) CZC-1.9, (d) CZC-1.4, (e) CZC-1.2

Zn/Cr ratio and the spectra are anisotropic with clearly defined  $g_{\parallel}$  and  $g_{\perp}$  regions as expected for Cu<sup>2+</sup> ions in a surrounding with axial symmetry. The well-resolved hyperfine structure due to isolated Cu<sup>2+</sup> species appeared at  $g_{\parallel} = 2.355$ , and  $A_{\parallel} = 12.1$  mT, and the unresolved pattern at  $g_{\perp} = 2.104$  and  $A_{\perp}$  over CZC-6.8 and CZC-3.3 catalysts. These experimental results are in good agreement with the reported literature [35–37]. At low Zn/Cr ratios (Fig. 5c, d) the peaks are broadened and shifted to higher values and the broad signals are probably due to the Cr<sup>3+</sup> species present in the catalyst [38]. The broad ESR signal of Cr<sup>3+</sup> can be due to CuCr<sub>2</sub>O<sub>4</sub> species [39], which is observed at low Zn/Cr ratios in XRD analysis. This result suggests the  $g_{\parallel}$  region, which is ascribed to isolated Cu<sup>2+</sup> species and is disappeared over the catalysts with low Zn/Cr ratios while the  $g_{\perp}$  region, ascribed to the Cr<sup>3+</sup> species, appeared. It could be explained as to the participation of some part of Cu<sup>2+</sup> ions in the formation of an oxide complex and/or a copper chromate particularly over CuO–ZnO–Cr<sub>2</sub>O<sub>3</sub> with Zn/Cr = 1.2 and the XRD analysis showed CuCr<sub>2</sub>O<sub>4</sub> phase supporting this explanation [40]. Lack of hyperfine structure (Fig. 5c–e) at low Zn/Cr ratios is due to the CuO cluster formation that is also demonstrated in (Fig. 3) XRD analysis. Signals due to Cr<sup>5+</sup> species could not be seen in all the samples.

The ESR patterns of the used catalysts are shown in Fig. 6. Highly symmetrical broad signals, attributed due to Cr<sup>3+</sup> centered at 328.0 mT with corresponding  $g = 1.97$ , are observed the peaks with line widths of 56.4, 61.9, 59.9, 52.9, 43.0 mT for Cu–Zn–Cr of Zn/Cr = 6.8, 3.3, 1.9, 1.33, 1.2 catalysts respectively [41]. These Cr<sup>3+</sup> species are ascribed due to the presence of ZnCr<sub>2</sub>O<sub>4</sub> in the catalyst and it is unlikely that these species belong to CuCr<sub>2</sub>O<sub>4</sub> since XRD patterns of the used catalysts did not show any peaks due to CuCr<sub>2</sub>O<sub>4</sub> phase. Cu<sup>2+</sup> signals are not observed in

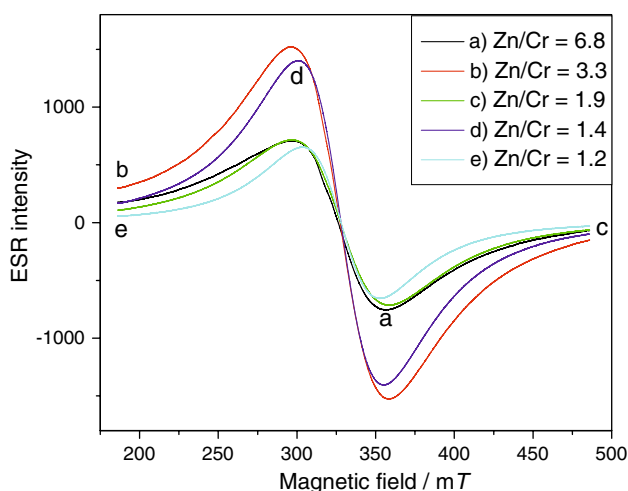


**Fig. 6** The ESR spectra of the used catalysts; (a) CZC-6.8, (b) CZC-3.3, (c) CZC-1.9, (d) CZC-1.4, (e) CZC-1.2

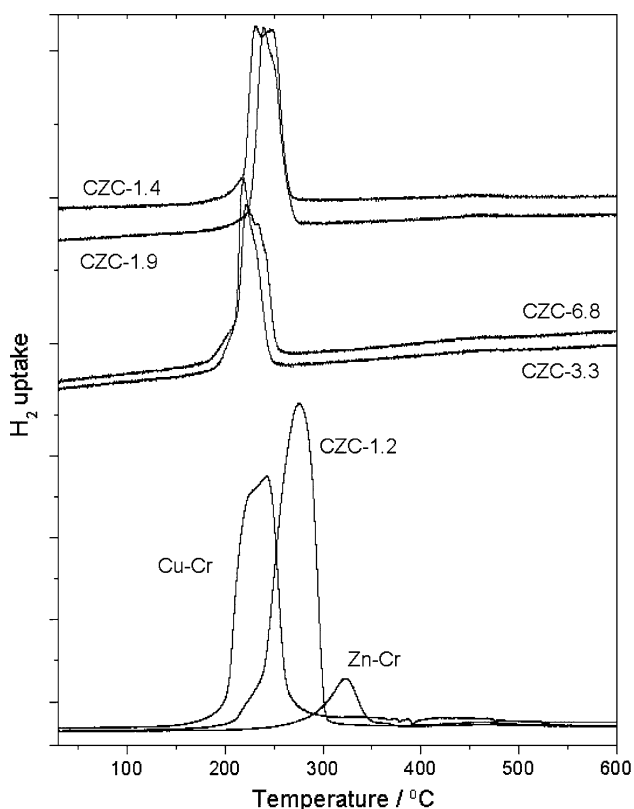


**Fig. 7** The TPR profiles of the fresh calcined Cu–Zn–Cr catalysts used catalysts indicating that all Cu<sup>2+</sup> species are in the reduced form.

### 3.4 Temperature Programmed Reduction (TPR)

The temperature programmed reduction profiles of the fresh catalysts are shown in Fig. 7. The CuO/Cr<sub>2</sub>O<sub>3</sub> sample

showed a reduction peak ( $T_{\max} \sim 230$  °C) with a shoulder and the ZnO/Cr<sub>2</sub>O<sub>3</sub> sample showed a single reduction peak at 325 °C. These results indicate that copper oxide in the proximity of chromium particles undergoes reduction below 270 °C and the chromium oxide in the proximity of zinc oxide particles completely was reduced at 350 °C.

It is also observed that the copper oxides in Cu–ZnO–Cr<sub>2</sub>O<sub>3</sub> samples are reduced in three stages and these peaks are presumably due to dispersed copper oxide, CuO interacted with ZnO or ZnCr<sub>2</sub>O<sub>4</sub> phase and the clustered CuO. The reduction peak is slightly shifted toward high temperatures with an increase in Cr content. The small reduction peak at the temperature below 200 °C can be assigned to the finely dispersed CuO. The dispersed Cu<sup>2+</sup> is reduced at temperatures lower than the clustered/bulk CuO species [42]. The intensity of the peak at the temperature below 200 °C is clearly observed to be high with CZC-6.8 and CZC-3.3 catalyst, while it is too little with CZC-1.4 and CZC-1.9 catalysts. In ESR analysis, the isolated Cu<sup>2+</sup> species are observed with CZC-6.8 and CZC-3.3 catalysts, but disappeared with CZC-1.4 and CZC-1.9 catalysts. The peak at about 220 °C is due to sequential reduction of bulk Cu<sup>2+</sup> into Cu<sup>0</sup> and the peak at 249 °C is probably due to strongly interacted copper oxide either with ZnO or ZnCr<sub>2</sub>O<sub>4</sub> phase. The shift in reduction peak towards high temperatures (Fig. 7) with an increase in chromium content (at low Zn/Cr ratios) indicates the formation of large CuO cluster as also evidenced in the XRD analysis (Fig. 3).

### 3.5 N<sub>2</sub>O Titrations

The copper metal surface areas of the fresh catalysts measured by N<sub>2</sub>O titrations are reported in Table 1. The Cu/ZnO/Cr<sub>2</sub>O<sub>3</sub> samples with the high Zn/Cr ratio showed copper metal surface areas higher than the samples with low Zn/Cr ratio. From this it is reasonable to note that CZC-3.3 ( $S_{\text{Cu}} = 6.5$  m<sup>2</sup>/g) and CZC-6.8 ( $S_{\text{Cu}} = 5.2$  m<sup>2</sup>/g) catalysts produce finely dispersed copper on the catalyst surface. The Cu metal surface areas of CZC-1.2, CZC-1.4 and CZC-1.9 with low Zn/Cr ratio are 0.92, 1.44 and 2.6 m<sup>2</sup>/g, respectively. The high copper metal surface areas of CZC-3.3 and CZC-6.8 can also be supported from the ESR analysis (Fig. 5a, b). The strong axially symmetrical signals over CZC-3.3 and CZC-6.8 catalysts at  $g_{\parallel} = 2.35$  are generally attributed to highly dispersed or isolated Cu<sup>2+</sup> species interacted with support material. As shown in Fig. 4, the broad reflections of CuO and ZnO phases over CZC-3.3, CZC-6.8 catalysts suggest that copper particles are in intimate contact with ZnO matrix [43]. On the contrary, XRD patterns of CZC-1.2, CZC-1.4 and CZC-1.9 catalysts showed (Fig. 3) sharp CuO peaks which can be assigned to the CuO cluster, which is also evidenced from

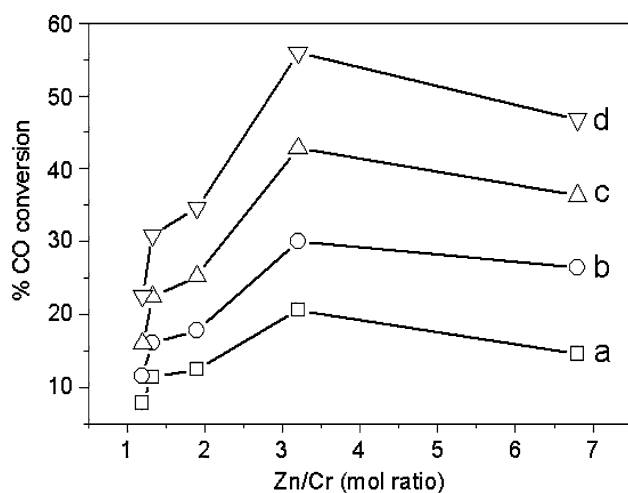


**Fig. 8** The CO conversion over Cu–Zn–Cr catalysts with respect to the Zn/Cr ratio at the temperature of (a) 240 °C, (b) 250 °C, (c) 260 °C, (d) 270 °C

the asymmetrical peaks with narrow line width and the disappearance of isolated  $\text{Cu}^{2+}$  species in the  $g_{\parallel} = 2.35$  region as shown in Fig. 5 (ESR analysis). From this observation, it can be concluded that ZnO plays an important role to disperse copper on the catalyst surface by increasing the isolated  $\text{Cu}^{+2}$  in the calcined samples.

### 3.6 Activity Measurements

The temperature dependence on CO hydrogenation activities are reported in Fig. 8. Increase in reaction temperature increased CO conversion was up to 270 °C over all the catalysts. The catalysts showed higher CO conversions at high Zn/Cr ratios and maximum is found over the catalyst with Zn/Cr = 3.3. The STD synthesis rate is proportional to the copper metal surface areas of the catalysts as observed from Fig. 1. The selectivity towards DME is  $\sim 70$  and 30% towards  $\text{CO}_2$  over all the catalysts. The activities of Zn–Cr and Cu–Cr catalysts are tested under the above reaction conditions at 270 °C. The CO conversions on Zn–Cr and Cu–Cr catalysts are found to be less than 1% and  $\text{CO}_2$  is the only product observed.

## 4 Discussion

From Table 1, it is clearly evident that CZC-3.3 is found to have higher copper metal surface area over the other catalysts. It appears that the optimum Zn/Cr ratio for high syngas conversion lies between 3.2 and 6.8 in this case which is also evidenced from the ESR analysis at low chromium contents; isolated/dispersed  $\text{Cu}^{2+}$  peaks are

predominant than at high chromium loadings. It is also evident that at low Zn/Cr ratios isolated  $\text{Cu}^{2+}$  signals disappeared (Fig. 5d, e) with the evolution of broad ESR signals attributed to clustered  $\text{Cu}^{2+}$  species. Unfortunately, at present we have no direct experimental evidence showing how these  $\text{Cu}^{2+}$  species can contribute to the CO hydrogenation activity. However, the disappearance of isolated  $\text{Cu}^{2+}$  (dispersed CuO) in high chromium loaded catalysts demonstrated the low CO conversions in contrast to the low Cr loaded CZC-3.3 and CZC-6.8 catalysts. From this it can be concluded that isolated copper species play an important role during syngas conversions. XRD analysis of these catalysts revealed that sharp diffraction lines due to CuO at high chromium loadings (Fig. 3) as well as the  $\text{CuCr}_2\text{O}_4$  phase although in minor intensity only in CZC-1.2 catalyst. On the contrary as aforesaid at high Zn/Cr ratios the CuO and ZnO peaks are not resolved and increase in ZnO lines observed; eventually the diffraction lines are broad, which indicates the close contact between copper and zinc particles. This suggests that interaction between copper and zinc particles are necessary in order to achieve high syngas conversions. Another factor that supports our results is based on the good agreement of copper metal surface areas (Table 1) against syngas conversions.

The XRD patterns of the used catalysts showed the decrease in peak intensities due to  $\text{CuCr}_2\text{O}_4$  phase however, the  $\text{ZnCr}_2\text{O}_4$  peaks remained intact. The used catalysts are obtained after reductive pretreatment with 5%  $\text{H}_2/\text{Ar}$  at 280 °C and subsequent syngas exposure at 240–270 °C for prolonged time and subsequently passivated in  $\text{N}_2$  atmosphere. The syngas reaction at 270 °C and reduction temperature i.e. 280 °C is sufficient enough to completely reduce the  $\text{CuCr}_2\text{O}_4$  species and complete reduction of  $\text{ZnCr}_2\text{O}_4$  seems unlikely at temperature below 280 °C. Hence, the intensities of the diffraction lines due to  $\text{CuCr}_2\text{O}_4$  peaks decreased and those of the  $\text{ZnCr}_2\text{O}_4$  peaks remained the same in the used samples. This observation is in good agreement with the TPR analysis where reduction of Zn–Cr sample occurred at high temperatures i.e. 350 °C.

The low syngas conversions at high chromium loadings is attributed to the formation of  $\text{CuCr}_2\text{O}_4$  and the role of  $\text{ZnCr}_2\text{O}_4$  appears to enhance the copper dispersion as observed from high copper metal surface areas over the samples with high Zn/Cr ratios i.e. CZC-3.3 and CZC-6.8 catalysts. Even if there was no observable difference in the XRD and ESR data obtained for  $\text{Cu}^{2+}$ , similar change is expected to take place on the surface of the catalyst, where isolated/dispersed  $\text{Cu}^{2+}$  species are significantly higher over high Zn/Cr catalysts which is further supplemented from the  $\text{N}_2\text{O}$  titrations, in other words at higher Zn loading the  $\text{Cu}^{2+}$  is highly dispersed or stabilized on the catalyst surface and high syngas conversions are obtained [44].

## 5 Conclusions

The Cu–Zn–Cr LDH precursors are synthesized (keeping copper content constant and varying the Zn/Cr ratios in order to see the influence of both Zn and Cr on the dispersion of copper), characterized and evaluated for syngas conversions. Based on the results obtained the following conclusions are drawn.

At high Zn/Cr ratios the XRD analysis of the fresh calcined catalysts disclosed the unresolved diffraction lines of CuO and ZnO attributed to intimate contact between copper and zinc particles. ESR analysis indicated the isolated Cu<sup>2+</sup> signals at high Zn/Cr ratios in the  $g_{||} = 2.35$  region, which disappeared at low Zn/Cr samples presumably due to the formation of CuCr<sub>2</sub>O<sub>4</sub> phase. The TPR profiles showed that reduction peak due to Cu<sup>2+</sup> shifted to high temperatures with increase in chromium loading suggesting the formation of large copper crystallites, which is also evidenced from the XRD analysis. The diffraction lines due to metallic copper, ZnO phases in major and ZnCr<sub>2</sub>O<sub>4</sub> in minor intensities are observed in the used catalysts. The ESR analysis gave supporting evidence due to the presence of only Cr<sup>3+</sup> species since the Cu<sup>0</sup> is ESR inactive. It appears that isolated copper species play an important role on syngas conversion and ZnCr<sub>2</sub>O<sub>4</sub> seems to disperse the copper on the catalyst surface. Finely dispersed copper particles are obtained at Zn/Cr mole ratio = 3.3 as evident from the high copper metal surface area over CZC-3.3 catalyst at a ca. 6.5 m<sup>2</sup>/g obtained by N<sub>2</sub>O titrations. The optimum Zn/Cr mole ratio lies between 3.3 and 6.8 and high syngas conversion is obtained over catalyst with Cu:Zn:Cr = 7:6:1.88 (mol ratios) catalyst. The high syngas conversion over Cu–Zn–Cr with Zn/Cr = 3.3 catalyst is attributed to the high copper metal surface area as compared to the other catalysts. Finally it can be concluded that higher yields of DME is obtained in single step over a composite catalyst comprised of finely mixed Cu–Zn–Cr (Zn/Cr = 3.3) with  $\gamma$ -Al<sub>2</sub>O<sub>3</sub>.

**Acknowledgments** This work is financially supported by a program of Energy and Resources Technology Development. One of the authors AV acknowledges the KOFST, (Korea) for financial support and Director-IICT, Hyderabad and CSIR-New Delhi, India.

## References

- Fujimoto K, Asami K, Shikada T, Tominaga H (1984) Chem Lett 2051
- Hansen JG, Voss B, Joensen F, Siguroardottir ID (1995) SAE Technical Paper Series 950063
- Klier K, Chatikavanij V, Herman RG, Simmons GW (1982) J Catal 74:343
- Fleisch TH, Mievil RL (1984) J Catal 90:165
- Busetto C, Del Piero G, Manara G, Trifiro F, Vaccari A (1984) J Catal 85:260
- Campos-Martin JM, Guerrero-Ruiz A, Fierro JLG (1995) J Catal 156:208
- Kim JH, Park M, Joo OS, Jung KD (2004) Appl Catal 264:37
- Frost JC (1988) Nature 334:557
- Klier K (1982) Adv Catal 31:243
- Bartley GJJ, Burch R (1988) Appl Catal 43:141
- Joo OS, Jung KD, Han SH, Uhm SJ (1995) J Catal 157:259
- Joo OS, Jung KD, Han SH, Uhm SJ, Lee DK, Ihm SK (1996) Appl Catal 135:273
- Fischer IA, Bell AT (1998) J Catal 178:153
- Spencer MS (1998) Catal Lett 50:101
- Miller GJ, Rochester CH, Bailey S, Waugh KC (1992) J Chem Soc Faraday Trans 88:2085
- Chinchen GC, Waugh KC, Whan DA (1986) Appl Catal 25:101
- Bart JCJ, Sneed RPA (1987) Catal Today 2:1
- Burch R, Golunski SE, Spencer MS (1990) J Chem Soc Faraday Trans 86:2683
- Denise B, Sneed RPA, Beguin B, Cherifi O (1987) Appl Catal 30:353
- Fisher IA, Woo HC, Bell AT (1997) Catal Lett 44:11
- Kiennemann A, Irdri H, Hindermann J, Lavalley J, Vallet A, Chaumette P, Courty P (1990) Appl Catal 59:165
- Spencer MS (1987) Surf Sci 192:336
- van Herwijnen T, de Jong WA (1974) J Catal 34:209
- Jung KD, Joo OS, Han SH, Uhm SJ, Chung IJ (1995) Catal Lett 35:303
- Jung KD, Joo O-S (2002) Catal Lett 84:21
- Klopprogge JT, Hickey L, Frost RL (2005) Mater Chem Phys 89:99
- Evans JW, Wainwright MS, Bridgewater AJ, Young DJ (1983) Appl Catal 7:75
- Robinson WRAM, Mol JC (1990) Appl Catal 60:73
- Porta P, Morpurgo S (1995) Appl Clay Sci 10:31
- Morpurgo S, Jacano ML, Porta P (1995) J Solid State Chem 119:246
- Frost RL, Ding Z (2003) Thermochim Acta 405:207
- Trifiro F, Vaccari A, Piero GD (1988) In: Unger KK, Raoquerol J, Sing KSW, Kral H (eds) Characterization of porous solids. Elsevier, Amsterdam, p 571
- Terlecki-Baricevic A, Jovanovic D, Grbic B, Marinova T, Kirilov-Stefanov P (1994) Appl Catal A: Gen 108:115
- Wang Z, Liu Q, Yu J, Wu T, Wang G (2003) Appl Catal A: Gen 239:87
- Sakata S, Nakai T, Yahiro H, Shiotani M (1997) Appl Catal A: Gen 165:467
- Tanabe T, Iijima T, Koiwai A, Mijuno J, Yokota K, Isogai A (1995) Appl Catal B: Environ 6:145
- Bahranowski K, Dula R, Gasior M, Labanowski M, Michalik A, Vartikian LA, Serwicka EM (2001) Appl Clay Sci 18:93
- Poole CP Jr, Kehl WL, MacIver DS (1962) J Catal 1:407
- Wojciechowska M, Haber J, Lomnicki S, Stoch J (1999) J Mol Catal A: Chem 141:155
- Lee CY, Jung TH, Ha BH (1996) Appl Catal B: Environ 9:77
- Ralek M, Gunsser W, Knappwost A (1968) J Catal 11:317
- Campos-Martin JM, Fierro JLG, Guerrero-Ruiz A, Herman RG, Klier K (1996) J Catal 163:418
- Robinson WRAM, Mol JC (1990) Appl Catal 60:61
- Huang X, Ma L, Wainwright MS (2004) Appl Catal A: Gen 257:235